HHS Public Access

Author manuscript

ACS Appl Mater Interfaces. Author manuscript; available in PMC 2018 January 12.

Published in final edited form as:

ACS Appl Mater Interfaces. 2018 January 10; 10(1): 127–138. doi:10.1021/acsami.7b13750.

Multifunctional Copper-Containing Carboxymethyl Chitosan/Alginate Scaffolds for Eradicating Clinical Bacterial Infection and Promoting Bone Formation

Yao Lu[†,‡], **Lihua Li**[‡], **Ye Zhu**[§], **Xiaolan Wang**[‡], **Mei Li**[‡], **Zefeng Lin**[‡], **Xiaoming Hu**[†,‡], **Yu Zhang**[‡], **Qingshui Yin**[†,‡,*], **Hong Xia**[†,‡,*], and **Chuanbin Mao**[§,‖,*]

[†]Southern Medical University, No. 1023 Shatai Road, Guangzhou, Guangdong 510515, China

[‡]Guangdong Key Lab of Orthopedic Technology and Implant Materials, Key Laboratory of Trauma & Tissue Repair of Tropical Area of PLA, Department of Orthopedics, Guangzhou General Hospital of Guangzhou Military Command, No. 111 Liuhua Road, Guangzhou, Guangdong 510010, China

[§]Department of Chemistry and Biochemistry, Stephenson Life Sciences Research Center, University of Oklahoma, Norman, Oklahoma 73072, United States

[‖]School of Materials Science and Engineering, Zhejiang University, Hangzhou, Zhejiang 310027, China

Abstract

Repairing infected bone defects relies on a scaffold that can not only fill the defects to promote bone formation but also kill clinically present bacterial pathogens such as *Staphylococcus aureus* (*S. aureus*). To meet this demand, here, we develop a new copper (Cu) containing natural polymeric scaffold with a full potential for repairing infected bone defects. Instead of directly adding antibacterial Cu^{2+} ions to the polymer mixtures, which caused uncontrolled polymer cross-linking, we added Cu nanoparticles to the mixture of anionic carboxymethyl chitosan (CMC) and alginate (Alg). Then, the Cu^{2+} ions released from the Cu nanoparticles gradually cross-linked the polymer mixtures, which was further turned into a scaffold (CMC/Alg/Cu) with an interconnected porous structure by freeze-drying. We found that the CMC/Alg/Cu scaffolds showed significantly improved capabilities of osteogenesis and killing clinical bacteria compared to CMC/Alg scaffolds fabricated by the same procedure but without adding Cu nanoparticles. Specifically, *in vitro* studies showed that the CMC/Alg/Cu scaffolds with excellent biocompatibility could enhance preosteoblastic cell adhesion by upregulating the expression level of adhesion-related genes (focal

[*]Corresponding Authors: gz_yqs@126.com (Q.Y.), gzxiahong2@126.com (H.X.), cbmao@ou.edu (C.M.).

ORCID

Chuanbin Mao: 0000-0002-8142-3659

Notes

The authors declare no competing financial interest.

Supporting Information

The Supporting Information is available free of charge on the ACS Publications website at DOI: 10.1021/acsami.7b13750. SEM image of the Cu-containing CMC/Alg scaffolds made with Cu^{2+} ions alone (CMC/Alg/Cu ions scaffold); cytotoxicity of the CMC/Alg/Cu ions scaffolds; short-term and long-term cytotoxicity of the CMC/Alg/Cu scaffolds made with different concentrations of Cu nanoparticles; antibacterial property of the CMC/Alg/Cu scaffolds made with different concentrations of Cu nanoparticles *in vitro* (PDF)

adhesion kinase (FAK), paxillin (PXN), and vinculin (VCL)), promoting osteogenic differentiation and mineralization by upregulating the osteogenesis-related gene expression and extracellular calcium deposition. *In vivo* studies further demonstrated that CMC/Alg/Cu scaffolds could induce the formation of vascularized new bone tissue in 4 weeks while avoiding clinical bacterial infection even when the implantation sites were challenged with the clinically collected *S. aureus* bacteria. This work represents a facile and innovative approach to the fabrication of Cu containing polymer scaffolds that can potentially be used to repair infected bone defects.

Graphical abstract

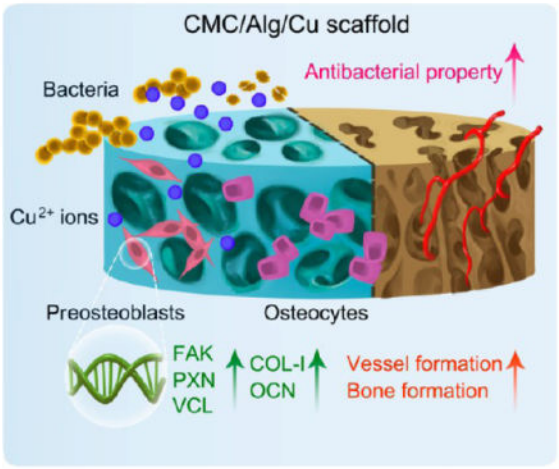

Keywords

carboxymethyl chitosan; alginate; nanoparticles; bacterial infection; infected bone defect

1. INTRODUCTION

Open fracture is one of most common injuries in orthopedics. The incidence of high-energy injuries and related open fractures continues to rise and is becoming a growing worldwide health concern.[1] This type of injury often causes complications such as bone defects and bacterial infection. Hence, infected bone defects remain a clinical challenge.[2] To treat these defects, ideally, a scaffold needs to be implanted to fill the defect to promote new bone formation and at the same time should be able to kill clinically present bacteria. Hence, there is a pressing need for the development of an osteogenesis-inducing and clinical bacteria-killing scaffold.

Natural polymers are potential candidates for developing such scaffolds because they can be manufactured with active agents that promote bone regeneration and prevent bacterial infection simultaneously. Chitosan (CS) is a biocompatible natural cationic polymer with important biofunctions such as antitumoral, antimicrobial, and antioxidant activities.[3–6] However, CS is water insoluble. In order to improve its water solubility, strategies like carboxymethylation are implemented.[7,8] For example, carboxymethyl chitosan (CMC) has good water solubility and biocompatibility.[9,10] Alginate (Alg) is another biocompatible

natural polymer and is studied for bone tissue engineering next to CS.[11–13] Although many CS/Alg-based scaffolds have been developed for bone tissue engineering, such as CS/Alg/hydroxyapatite, CS/polypyrrole/Alg, and CS/Alg/fucoidan scaffolds,[14–16] most of them are geared to promoting bone formation as filling materials but very few are designed with the additional function of killing clinically present bacteria for repairing infected bone defects.

Within recent years, some materials with an antibacterial property have been successfully fabricated, mainly by loading antibiotics.[17–19] However, there are still limitations in the antibiotic-loading materials, such as short antibiotic release duration as well as inconsistent bone formation.[20] Moreover, infected bone defects can hardly be cured by antibiotics, and abundant use of antibiotics often results in the appearance of more deadly multidrug resistant bacteria, namely, the “super-bugs.”

Copper (Cu) is a cheap and abundant resource on earth and is well-known for its strong broad-spectrum antibacterial activity. Cu is also an essential trace element in the human body and enhances bone formation.[21,22] Although Cu^{2+} ions were found to be antibacterial, previous antibacterial assays[23,24] were mainly performed on the nonclinically collected standard bacterial strains (e.g., *E. coli* ATCC25922) but not on the clinically collected deadly bacteria (e.g., *Staphylococcus aureus* (*S. aureus*)) with much stronger pathogenicity. Moreover, the influence of Cu^{2+} ions on the cell behavior, especially cell adhesion, has not been well studied. Furthermore, we found that adding Cu^{2+} solution directly to the anionic polymer solution led to immediate spontaneous cross-link of the natural polymers (Figure 1a–iii,vi), consistent with the earlier finding that it was difficult to prepare natural polymer scaffolds with homogeneous distribution of Cu^{2+} ions.[22]

In the present study, we developed a novel CMC/Alg/Cu scaffold with a facile method by using Cu nanoparticles as a source for Cu^{2+} ions instead of directly adding Cu^{2+} ions with the polymer mixture. Toward this goal, Cu nanoparticles were mixed with CMC and Alg to form a solution, which was frozen and further freeze-dried to form CMC/Alg/Cu scaffolds (Figure 1a). Cu^{2+} ions released from the Cu nanoparticles along with the additional Ca^{2+} ions gradually facilitated the electrostatic cross-linking of anionic polymers prior to freeze-drying, which favored the scaffold formation. Cu nanoparticles are relatively chemically stable and release Cu^{2+} ions gradually in solution,[25] which solved the aforementioned immediate spontaneous polymer cross-linking problem (Figure 1a). We found that the resultant CMC/Alg/Cu scaffolds are better than the CMC/Alg scaffolds (formed under the same procedure but in the absence of Cu nanoparticles) in terms of osteogenesis and antibacterial properties. Consequently, the CMC/Alg/Cu scaffolds could be used to fill the infected bone defects and kill the clinically derived bacteria associated with the defects.

2. EXPERIMENTAL SECTION

2.1. Preparation of CMC/Alg/Cu and CMC/Alg Scaffolds

Cu nanoparticles (Sigma, 10–30 nm, 0.635 mg) were added into 10 mL of deionized (DI) water. The mixture was stirred to gain a Cu nanoparticle solution. 150 mg of CMC powder (Macklin) and 150 mg of Alg powder (Sigma) were successively added into the Cu nanoparticle solution under constant stirring to form a homogeneous solution. The mixture

was then poured into 48-well plates and frozen overnight at −80 °C. Next, the mixture was freeze-dried in a lyophilizer (Q150T ES, QUORUM) until dried. The scaffolds were cross-linked with 2% $CaCl_2$ solution and washed with deionized (DI) water to remove unbound $CaCl_2$. Finally, the scaffolds were freeze-dried again, kept dry, and sterilized by epoxyethane. CMC/Alg scaffolds were fabricated in the same manner but in the absence of Cu nanoparticles in the initial CMC/Alg mixed solution.

2.2. Characterization of Prepared Scaffolds

2.2.1. Scanning Electron Microscopy (SEM)—The surface morphology and pore size of the scaffolds were examined using scanning electron microscopy (Nova NanoSEM 430, FEI). Scaffold samples were dried under vacuum, gold coated, and examined with SEM.

2.2.2. Fourier Transform-Infrared Spectroscopy (FTIR)—FTIR was used to examine intermolecular interaction between the components in the scaffolds. The spectra of CMC, Alg, CMC/Alg/Cu scaffolds, and CMC/Alg scaffolds were recorded using the KBr pellet method in an FTIR spectrophotometer (VERTEX 70, Bruker) with the range of 4000 to 500 cm^{-1}.

2.2.3. Swelling Behavior—The fluid uptake ability of the scaffolds was evaluated. The dry weight of the scaffolds was recorded. The scaffolds were immersed in phosphate buffer saline (PBS) at 37 °C. Their wet weight was recorded after they were taken out and removed by a filter paper. The swelling ratio was determined by using eq 1.

$$\text{swelling ratio} = (\text{wet weight} - \text{dry weight})/\text{dry weight} \quad (1)$$

2.2.4. Release of Cu^{2+} Ions—To determine the release of Cu^{2+} ions from the scaffolds, 20 mg of CMC/Alg/Cu scaffolds were placed in a tube and 1 mL of PBS was added. The tube was put on a shaker at room temperature. After 100 μL of liquid containing no scaffold was taken from the tube, the liquid sample was analyzed using an inductively coupled plasma atomic mass spectrometer (ICP-MS) (Agilent 7700x, Agilent Technologies) to quantify the amount of Cu^{2+} ions. Another 100 μL of PBS was supplemented into the tube after collection. The same procedure was repeated at 5 and 30 min and 1, 3, 5, 7, 12, and 24 h.

2.3. In Vitro Studies

2.3.1. Cell Proliferation—Cell Counting Kit-8 (CCK-8) assay was used to determine the cell proliferation. Scaffolds weighing 10 mg were placed in the plates. A 500 μL suspension of MC3T3-E1 preosteoblastic cells with the concentration of 1×10^5 cells/mL was seeded and incubated with the scaffolds at 37 °C. The α-Minimum Essential Medium (α-MEM, Gibco), supplemented with 10% fetal bovine serum (FBS, Gibco), was removed on the respective days. After the cells were cultured for 1, 3, and 7 days, the media were drained. 500 μL of CCK-8 solution (10%) was added to each well and incubated for 2 h. Optical

densities (ODs) were determined at 450 nm using a microplate reader (Multiskan GO, Thermo Scientific). Each experiment was performed in triplicate.

2.3.2. Hemolysis Tests—Healthy human blood was collected and diluted with normal saline in a ratio of 4:5 by volume. CMC/Alg/Cu scaffolds and CMC/Alg scaffolds were dipped in 1 mL of normal saline and incubated at 37 °C for 30 min. One mL of deionized water and PBS was set as a positive control and negative control, respectively. Then, 0.2 mL of diluted blood was added into each sample, and the mixtures were incubated at 37 °C for 1 h. After that, all samples were centrifuged for 5 min at 1690*g* and the supernatant was collected. The OD of the supernatants was determined to be 545 nm using the microplate reader. The percentage of hemolysis was calculated using the following eq 2, where control(+) and control(−) represent the positive and negative control, respectively.

$$\text{hemolysis rate}\,(\%)=(\mathrm{OD}_{\text{scaffold}}-\mathrm{OD}_{\text{control}(-)})/(\mathrm{OD}_{\text{control}(+)}-\mathrm{OD}_{\text{control}(-)})\times 100 \quad (2)$$

Each experiment was performed in triplicate.

2.3.3. Cell Adhesion—SEM was used to observe cell adhesion in the scaffolds. After being cultured for 24 h, the scaffolds loaded with MC3T3-E1 cells were washed with PBS and then fixed with 3% glutaraldehyde for 4 h in 4 °C. The scaffolds were dehydrated in a graded ethanol series (30%, 50%, 70%, 90%, and 100%, respectively). The cell loaded scaffolds were dried under vacuum, gold coated, and examined with SEM (Ultra 55, ZEISS).

2.3.4. Cytoskeleton Staining and Cell Distribution—The scaffolds loaded with MC3T3-E1 cells were washed with PBS after 24 h of culture. The cells were permeabilized with 0.1% Triton X-100 for 4 min at room temperature followed by washing with PBS. Then, the cells were stained with Actin red (KeyGEN BioTECH) at room temperature for 1 h and DAPI (Sigma) for 10 min. The cytoskeletal actin and cell nuclei were examined by confocal laser scanning microscopy (LSM 700, ZEISS).

2.3.5. Adhesion-Related Genes Expression—The expressions of adhesion-related genes were evaluated by real-time quantitative polymerase chain reaction (RT-qPCR). MC3T3-E1 cells were seeded in 10 mg scaffolds and cultured for 24 h. The total RNA of the cultured osteoblasts was isolated using a TRIZOL reagent (Invitrogen). Chloroform was added to isolate the RNA into the aqueous phase. The upper colorless aqueous phase was transferred to a new 1.5 mL tube, and the isopropanol was added to precipitate the RNA. Finally, the RNA pellets were washed with 75% ethanol and dissolved in the RNase inhibitor diethyl pyrocarbonate treated water. The RNA concentrations were determined on the Nanodrop 2000 spectrophotometer (Thermo Scientific). One mg of RNA from each sample was reverse transcribed into complementary DNA (cDNA) using the RNA-to-cDNA master mix kit (Applied Biosystem) by following the manufacturer's instructions. Expression level of genes including integrin $\alpha 5$ (ITGA5), integrin $\beta 1$ (ITGB1), focal adhesion kinase (FAK), paxillin (PXN), and vinculin (VCL) were quantified using Rotor-gene Q (Qiagen) with SYBR Premix Ex Taq II (TaKaRa). The cycling protocols were set as

follows: 95 °C for 15 min, followed by 45 cycles including 95 °C for 5 s and 60 °C for 30 s. The results were analyzed using the Rotor-Gene Real-Time analysis software 6.0. The relative mRNA expression level of each gene was normalized to the housekeeping gene glyceraldehyde-3-phosphate dehydrogenase (GAPDH) and determined using cycle threshold values. The forward and reverse primers of the selected genes were listed in Table 1. Each experiment was performed in triplicate.

2.3.6. Intracellular Total Protein and Alkaline Phosphatase (ALP) Activity— Osteogenic differentiation of MC3T3-E1 cells (5×10^4 cells) cultured in 10 mg scaffolds was analyzed after 7 and 14 days of culture in an osteogenic medium (Cyagen Biosciences). At each time point, the osteogenic medium was removed, washed twice with PBS, and lysed in 0.2% Triton X-100 for 12 h at 4 °C. The alkaline phosphatase (ALP) activities were determined by a colorimetric assay using an ALP reagent containing *p*-nitrophenyl phosphate (p-NPP, Sigma) as the substrate, and the absorbance of *p*-nitrophenol (p-NP) formed was measured at 405 nm. The concentrations of the proteins in the collected solutions were determined by a BCA protein assay kit (Pierce). The ALP activity was finally normalized to the total protein content correspondingly. Each experiment was performed in triplicate.

2.3.7. Extracellular Matrix Mineralization—The mineralization assay was performed by alizarin red S stain. MC3T3-E1 cells (5×10^4 cells) were cultured with 10 mg scaffolds. On day 14, the media were removed and washed twice by PBS. The scaffolds and cells were fixed in 4% polyformaldehyde for 30 min at room temperature and then washed by PBS. The scaffolds and cells were stained with alizarin red S (Cyagen Biosciences, pH= 8.3) for 5 min. They were washed with PBS for five times and then dissolved in 10% cetylpyridinium chloride in 10 mM sodium phosphate (pH= 7.0), and the OD value was measured at 620 nm. Each experiment was performed in triplicate.

2.3.8. Osteogenesis-Related Genes Expression—The expressions of osteogenesis-related genes were evaluated by RT-qPCR. MC3T3-E1 cells were seeded with 5×10^4 cells in 10 mg scaffolds and cultured for 7 and 14 days. The isolation and reverse transcription of RNA followed the same protocol described above. Expression levels of the osteogenesis-related genes including runt-related transcription factor 2 (RUNX2), type I collagen (COL-I), and osteocalcin (OCN) were quantified. GAPDH was used as the housekeeping gene. The forward and reverse primers of the selected genes were listed in Table 2. Each experiment was performed in triplicate.

2.4. *In Vivo* Studies

2.4.1. Preparation of MC3T3-E1 Cells Loaded Scaffolds—The scaffolds weighing 10 mg were placed in the plates. A 500 μL suspension of MC3T3-E1 cells with the concentration of 1×10^5 cells/mL was seeded and incubated with the scaffolds in the osteogenic media at 37 °C. The media was changed every 2 days until day 7 and then replaced by FBS free α-MEM.

2.4.2. Rat Ectopic Osteogenesis and Infection Model—All animal procedures were approved by the ethics committee of Guangzhou General Hospital of Guangzhou Military Commands. Adult Sprague–Dawley rats (250–300 g) were randomly divided into 2 groups with 6 rats in each group. The rats were anesthetized by intraperitoneal injection of 3% pentobarbital solution. Lower limbs were shaved and sterilized with iodine and ethanol and draped in a sterile manner. A 1 cm incision was made on the lateral thigh of the rat. The intermuscular spaces were bluntly dissected to expose the muscle pouch of the gluteus maximus. The MC3T3-E1 cells loaded CMC/Alg/Cu scaffolds were implanted, and 10 μL of clinical *S. aureus* (1×10^7 CFU/mL in PBS) was delivered into the muscle pouch. The incision was closed in two layers with nylon suture in subcutaneous tissues and skin, respectively. This procedure was repeated in the opposite limb of the same rat with a CMC/Alg scaffold implanted. Each rat was kept and observed in a separate cage after operation. The rats were euthanized with overdosed pentobarbitol (100 mg/kg) to harvest the implanted scaffolds 2 and 4 weeks after implantation.

2.4.3. Micro-CT Evaluation—After implantation of the scaffolds for 2 and 4 weeks, the rats were euthanized and the new bone formation in the scaffolds was detected with Micro-CT (Aloka). The scan parameters included a scanning resolution of 48 μm, a rotation angle of 360, and a voltage of 80 kV. The obtained CT images were transferred into three-dimensional (3D) reconstructed images by the bundled software. The bone mineral density (BMD, mg/cm^3) and total bone volume (TBV, mm^3) of the scaffolds were measured and analyzed.

2.4.4. Histological Assessment—The harvested samples were fixed with 4% polyformaldehyde overnight and dyed with hematoxylin and eosin staining (H&E), Giemsa staining, and Masson's trichrome staining, respectively. The histological morphology of the samples was observed under an inverted microscope (BX51, Olympus).

2.4.5. In Vivo Antibacterial Property—After being harvested, the samples were immediately rolled on the LB agar plates in a clean bench. The number of viable bacterial colonies was counted after incubation at 37 °C for 24 h.

2.5. Statistical Analysis

Analysis was performed using SPSS 19.0 software. *In vitro* studies were measured using one-way analysis of variance. *In vivo* studies were analyzed by the compared *t* test. $p < 0.05$ was regarded as significant difference.

3. RESULTS

3.1. Characterization of Prepared Scaffolds

The surface morphology and pore dimensions of the scaffolds were studied by SEM analysis. Figure 1b,c demonstrates that both scaffolds have a porous and interconnected structure. Well-distributed and well-defined pores were observed in the CMC/Alg/Cu scaffolds. The pore size of the CS/Alg/Cu scaffolds was 115.51 ± 13.63 μm. The pores of the CMC/Alg scaffolds were rough and irregular, with a pore size ranging from 45 to 107

μm and with an average of 73.06 ± 21.13 μm. We also observed the morphology of the Cu-containing CMC/Alg scaffolds made with Cu^{2+} ions alone and found that the porous structure in the resultant scaffolds was not as well distributed as in CMC/Alg/Cu scaffolds (Figure S1).

The FTIR spectra of the scaffolds and the individual components are shown in Figure 1d. The spectra of both scaffolds showed the characteristic peaks of CMC and Alg. The peaks of CMC and Alg at 1621 and 1623 cm^{-1} were replaced by new peaks of the scaffolds at 1627 and 1635 cm^{-1}, suggesting the polymer cross-link by Ca^{2+} and Cu^{2+} ions. Compared with CMC/Alg scaffolds, the characteristic peaks for carbonyl groups (–COOH and C═O) in the CMC/Alg/Cu scaffold were shifted and intensified from 1627 to 1635 cm⁻1 and from 1429 to 1433 cm^{-1}, respectively. Correspondingly, the peak for hydroxyl group (–OH) was also shifted and intensified from 3432 to 3426 cm^{-1}.

The fluid uptake ability of the scaffolds was measured by the swelling study in PBS solution. As Figure 1e shows, at the end of each incubation period, CMC/Alg/Cu scaffolds showed a decrease in the swelling ratio compared with CMC/Alg scaffolds.

Figure 1f shows the release of Cu^{2+} ions from the CMC/Alg/Cu scaffolds measured in PBS. The release of Cu^{2+} ions in the first 3 h was slow. During 5–12 h, the released amount of Cu^{2+} ions was significantly increased and then slowed down after 12 h.

3.2. *In Vitro* Study

3.2.1. Biocompatibility—First, we analyzed the cytotoxicity of Cu-containing CMC/Alg scaffolds made with 1 mmol/L Cu^{2+} ions alone and found that these scaffolds were cytotoxic (Figure S2). We also tested the short-term and long-term cytotoxicity of the Cu-containing CMC/Alg scaffolds made with different concentrations of Cu nanoparticles by the MTT assay. As shown in Figure S3, when the concentration of Cu nanoparticles was 10 mmol/L, the scaffolds significantly inhibited cell proliferation. However, the scaffolds made with 1 mmol/L Cu nanoparticles showed low cytotoxicity. Hence, the scaffolds with 1 mmol/L Cu nanoparticles were chosen for the further study. Then, the prepared CMC/Alg/Cu and CMC/Alg scaffolds were subjected to cell proliferation of MC3T3-E1 cells by the CCK-8 assay. The OD values of the prepared scaffolds at different time intervals are shown in Figure 2a. After 1 and 3 days of incubation, the CMC/Alg/Cu scaffolds showed no significant toxicity toward MC3T3-E1 cells compared with CMC/Alg scaffolds. The OD values and cell numbers increased along the culture time in these prepared scaffolds. A long-term CCK-8 assay was also performed for an incubation period of 7 days. The results demonstrated that the CMC/Alg/Cu scaffolds had no significant difference with CMC/Alg scaffolds, indicating that these scaffolds were noncytotoxic.

Figure 2b presents the hemolytic results of the prepared scaffolds. Positive control (DI water) showed a red solution in the tube due to the presence of released hemoglobin. Negative control (PBS) showed no red color in the tube indicating no hemolysis occurred. For the prepared scaffolds, the hemolysis of the CMC/Alg and CMC/Alg/Cu scaffolds was lower than 5% for both, suggesting that the scaffolds were almost not hemolytic to human red blood cells.

Cell adhesion in the scaffolds after 24 h of culture is shown in Figure 2c,d. In both scaffolds, the cells gathered together and grew in clusters. Filopodia of the cells were found to anchor to the surface of the scaffolds. However, cell morphology was different in the two types of the scaffolds. In the CMC/Alg scaffolds, the filopodia of the cells were not obvious, while they were longer and more typical in the CMC/Alg/Cu scaffolds. Cytoskeleton analysis (Figure 2e,f) also showed the difference in the cell morphology and that the expression of filamentous actin in the CMC/Alg/Cu scaffolds was higher than that in the CMC/Alg scaffolds.

Figure 2g shows the mRNA expression level of adhesion-related genes of MC3T3-E1 cells in the scaffolds after 24 h of culture. The expression level of ITGA5 had no difference between the two scaffolds while ITGB1 was significantly lower in the CMC/Alg/Cu scaffolds. FAK and VCL in the CMC/Alg/Cu scaffolds were significantly higher ($p < 0.01$) than in the CMC/Alg scaffolds. PXN was also higher in CMC/Alg/Cu scaffolds and almost reached a statistic difference ($p = 0.053$).

To explore the cell distribution in the scaffolds, MC3T3-E1 cell loaded scaffolds were examined by scanning laser confocal microscopy after 24 h of culture. As shown in Figure 2h, the cells were mainly concentrated in the upper layer of the CMC/Alg scaffolds, whereas they grew evenly throughout the CMC/Alg/Cu scaffolds.

3.2.2. Osteogenic Differentiation and Mineralization—ALP activity is a typical biochemical marker for osteoblastic activity and is used to assess the osteogenic differentiation of MC3T3-E1 cells in this study. Figure 3a shows the ALP activity of preosteoblasts in the scaffolds during the experimental period. These results showed that the ALP activity was significantly higher in the CMC/Alg/Cu scaffolds than in the CMC/Alg scaffolds on day 7 ($p = 0.027$). The expression of ALP in the scaffolds decreased from day 7 to day 14 because ALP is a marker for the early stage of osteogenesis.

Figure 3c shows the mRNA expression level of osteogenesis-related genes of MC3T3-E1 cells in the scaffolds after 7 and 14 days of culture. On day 7, the expression levels of RUNX2, COL-I, and OCN genes in the CMC/Alg/Cu scaffolds were higher than in the CMC/ALG scaffolds but not significant when compared with CMC/ALG scaffolds ($p =$ 0.428, 0.227, and 0.230, respectively). On day 14, the expression of RUNX2 had no difference between the CMC/Alg/Cu scaffolds and CMC/ALG scaffolds ($p = 0.942$) while COL-I and OCN were significantly higher in the CMC/Alg/Cu scaffolds than in CMC/ALG scaffolds ($p = 0.019$ and 0.027, respectively).

Alizarin red S staining is widely used for assaying the mineralization, the late stage of osteogenesis, due to its ability of selectively binding to calcium nodulation, a specific marker of extracellular mineralized deposit. The mineralization of the CMC/Alg/Cu and CMC/Alg scaffolds on day 14 is shown in Figure 3b. The mineralization was significantly increased in the CMC/Alg/Cu scaffolds as compared with CMC/Alg scaffolds ($p < 0.01$).

3.2.3. In Vitro Antibacterial Property—As shown in Figure S4, all the Cu-containing CMC/Alg scaffolds made with Cu nanoparticles showed an enhanced antibacterial property compared with the pure CMC/Alg scaffolds.

3.3. *In Vivo* Studies

3.3.1. Micro-CT evaluation—Figure 4a shows the 3D reconstructed micro-CT images of new bone formation in the scaffolds at weeks 2 and 4. Marked with red-dotted lines, new bone formation was observed 2 weeks after implantation in the CMC/Alg/Cu scaffolds and became much more obvious at week 4. However, bone formation was still negligible in the CMC/Alg scaffolds at week 4.

Figure 4b,c shows the bone mineral density (BMD, mg/cm^3) and total bone volume (TBV, mm^3) in the scaffolds. BMD and TBV were both increased along implantation time. At week 2, BMD was 235.74 ± 13.85 and 219.18 ± 11.13 mg/cm^3 and TBV was 24.53 ± 27.94 and 14.67 ± 16.00 mm^3, in the CMC/Alg/Cu and CMC/Alg scaffolds, respectively. At week 4, BMD was 310.86 ± 35.05 and 274.27 ± 22.68 mg/cm^3 and TBV was 41.97 ± 39.92 and 16.12 ± 12.29 mm^3 in the CMC/Alg/Cu and CMC/Alg scaffolds, respectively. BMD was significantly higher in the CMC/Alg/Cu scaffolds than in the CMC/Alg scaffolds after 2 and 4 weeks of implantation ($p < 0.05$). Although no statistic difference was achieved, there was a trend that TBV was higher in the CMC/Alg/Cu scaffolds than in the CMC/Alg scaffolds.

3.3.2. Histological Evaluation—*In vivo* compatibility of the scaffolds was assessed by hematoxylin and eosin (H&E) staining. Figure 5a shows the tissue response to the scaffolds at weeks 2 and 4 after implantation. At weeks 2 and 4, lobulated neutrophils (green arrows) migrating from circulating blood were observed in the CMC/Alg scaffolds due to the inflammation and injected *S. aureus*. However, no lobulated neutrophils were found in the CMC/Alg/Cu scaffolds. Moreover, osteocytes (blue arrows) could be found inside the scaffolds, and their number increased at week 4, suggesting a good tissue compatibility and osteogenic capability of the CMC/Alg/Cu scaffolds.

Figure 5b shows *S. aureus* and the related infection assessed by Giemsa staining. At week 2, *S. aureus* bacteria (yellow arrows) were seen in the CMC/Alg scaffolds, and then, the number of *S. aureus* bacteria decreased in the CMC/Alg scaffolds at week 4. No obvious *S. aureus* bacteria were found in the CMC/Alg/Cu scaffolds at both weeks 2 and 4.

Masson's trichrome staining was used to stain the formation of collagen and vascularization in the harvested scaffolds. As Figure 5c shows, collagen in blue (orange arrows) appeared in both scaffolds at week 2 and then increased throughout the scaffolds at week 4 after implantation. More collagen could be observed in the CMC/Alg/Cu scaffolds. Small blood vessels (red arrows) were found in the CMC/Alg/Cu scaffolds at week 2 postimplantation but not in the CMC/Alg scaffolds. It is noteworthy that there were more vessels formed in the CMC/Alg/Cu scaffolds than in the CMC/Alg scaffolds at week 4, which was also shown in the H&E staining (Figure 5a).

3.3.3. In Vivo Antibacterial Property—The results for *in vivo* antibacterial property of the CMC/Alg/Cu and CMC/Alg scaffolds are shown in Figure 6. At week 2, there were a

large amount of *S. aureus* colonies (229.33 ± 69.02) in the CMC/Alg scaffolds while there were only several colonies (2.67 ± 0.58) in the CMC/Alg/Cu scaffolds. The number of *S. aureus* colonies decreased at week 4. There were few *S. aureus* colonies (6 ± 5.72) in the CMC/Alg scaffolds while there were almost no colonies (1.67 ± 1.80) in the CMC/Alg/Cu scaffolds. These results showed the addition of Cu significantly reduced bacterial growth after 2 weeks of implantation ($p < 0.05$) and had a trend to reduce more bacterial growth after 4 weeks ($p = 0.089$).

4. DISCUSSION

4.1. Characterization of the Scaffolds

Cu doped scaffolds show promising multifunctional characteristics. However, Cu^{2+} solution acts as a cross-linking agent to cross-link polymers immediately and spontaneously during the preparation of natural polymeric materials. Moreover, the scaffolds made with Cu^{2+} ions alone were not satisfied in terms of the morphology (Figure S1) and biocompatibility (Figure S2). In this study, we fabricated Cu containing CMC/Alg scaffolds by using Cu nanoparticles as a precursor. Interestingly, we found that Cu nanoparticles were transformed into Cu^{2+} ions during fabrication, and Cu nanoparticles could be seen disappearing in the SEM image (Figure 1b). Previous studies have examined transformations in copper-based nanomaterials.[25,26] Mudunkotuwa et al. found that CuO shell could be formed around the Cu bulk core due to oxidation.[26] When immersed in PBS or culture medium, Cu nanoparticles would release Cu^{2+}ions. Thus, the gradually released Cu^{2+} ions make the CMC/Alg/Cu mixture remain homogeneous and flowable instead of immediately being cross-linked, enabling us to have a uniform precursor solution before freeze-drying for forming scaffolds.

During the preparation, we also found that the CMC/Alg/Cu solution gradually became more viscous. It suggested that the Cu^{2+} ions released from the Cu nanoparticles did act as a cross-linker between $–COO^-$ groups of CMC and Alg. However, the Cu^{2+} ions were not enough to cross-link all $–COO^-$ groups, and the remaining $–COO^-$ groups were later cross-linked by Ca^{2+} ions (Figure 1a). Cu^{2+} ions have a smaller ionic radius (and thus a larger charge density) than Ca^{2+} ions,[27] so the ionic bond with $–COO^-$ groups is stronger for Cu^{2+} ions than for the Ca^{2+} ions in the CMC/Alg/Cu scaffolds. It can be seen in the FTIR that the peaks for carboxyl, carbonyl, and hydroxyl groups were intensified in the CMC/Alg/Cu scaffolds compared with the CMC/Alg scaffolds (Figure 1). It has been shown that the repulsive force between ionized carboxyl groups is large enough to generate large pores in a scaffold.[28] Therefore, compared to the CMC/Alg scaffolds, CMC/Alg/Cu scaffolds are stable due to the presence of strong ionic bonds between Cu^{2+} ions and ionized carboxyl groups while bearing uniformly distributed large pores due to the large repulsive force between the ionized carboxyl groups (Figure 1).

4.2. Cell Adhesion and Biocompatibility

Cell–cell and cell–environment interactions are essential for tissue morphogenesis in embryonic skeletal development.[29] As illustrated in SEM results (Figure 1b,c), both of the prepared scaffolds had a highly porous and interconnected 3D structure. 3D environments

enhance cell condensation, cell–cell interactions, and cell biological activities.[30] Typical cell clusters and 3D growth were observed in both scaffolds. Interestingly, we found that the adhesion and cytoskeleton of MC3T3-E1 cells were better in the CMC/Alg/Cu scaffolds than in the CMC/Alg scaffolds. Integrin subunits are responsible for the initial adhesion of cells. The known receptors in integrin and their ligand can be bound by metal ions, for example, Mg^{2+}.[31] To the best of our knowledge, the effects of Cu^{2+} ions on the cell adhesion in the scaffolds have been little studied. Thus, we further examined the adhesion-related genes expression of the cells in both scaffolds after 24 h of culture. Generally, the cultured cells could adhere on the material surface within 4 h, and the expression of integrin genes decreased between 4 and 24 h.[32] The relatively lower expression of integrin α/β subunit genes (ITGA5 and ITGB1) after 24 h of culture suggested that the cells completed their adhesion in the CMC/Alg/Cu scaffolds earlier than in the CMC/Alg scaffolds. Then, the adhered cells began to proliferate and migrate, resulting in the higher expression of focal adhesion and actin cytoskeleton signaling pathway genes (FAK, PXN, and VCL). Activation of these signaling pathways can increase focal adhesion formation, regulate actin cytoskeleton structure, and promote cell spreading.[33] The distribution of the cells in the scaffolds after being cultured for 24 h also confirmed that the cells were more spread in the CMC/Alg/Cu scaffolds. Thus, the released Cu^{2+} ions in the CMC/Alg/Cu scaffolds enhanced cell adhesion as well as spreading by activating the focal adhesion and actin cytoskeleton pathway.

Cytotoxic effect is another important concern of biomaterials for tissue engineering. Chitosan and alginate are both natural polymers and nontoxic, but the addition of Cu may be toxic to mammalian cells. There is a general consensus that the cytotoxicity of Cu is attributed to the formation of dissolved Cu^{2+} ions and their oxidative pathways.[34–37] Our previous study demonstrates the best concentration of Cu^{2+} ions for maintaining high antibacterial efficacy but low cytotoxicity toward mammalian cells is 10^{-5} to 10^{-4} mol/L.[38] After considering both the cytotoxicity (Figure S3) and antibacterial property (Figure S4) of CMC/Alg/Cu scaffolds made with different concentrations of Cu nanoparticles, we determined that the scaffolds made with 1 mmol/L Cu nanoparticles exhibited a combination of very low cytotoxicity and high antibacterial property (above 99% bacterial reduction) *in vitro*. Hence, 1 mmol/L was chosen as the best concentration of Cu nanoparticles for producing CMC/Al/Cu scaffolds in this study. Moreover, the amount of Cu^{2+} ions (Figure 1f) released from the CMC/Alg/Cu made with this concentration of Cu nanoparticles was within the best concentration range of Cu^{2+} ions according to our previous research.[38] Hence, the prepared CMC/Alg/Cu scaffolds possessed good biocompatibility with no significant cytotoxic effect on MC3T3-E1 cells and no hemolysis to human red blood cells.

4.3. *In Vivo* Antibacterial Capability

The CMC/Alg/Cu scaffolds showed an excellent antibacterial capability toward clinical *S. aureus* bacteria compared with CMC/Alg scaffolds *in vivo*. In our previous study, we found that Cu^{2+} ions could cause a leakage of cellular materials by damaging the permeability of the outer membrane of the bacteria and inhibit cell respiration by producing a high level of reactive oxygen species (ROS).[39] Cu^{2+} ions were also found to interfere with the replication of *nuc* (species-specific) and 16S rRNA genes but with no damage to DNA.[39] Studies also

reported that Cu possessed an antibacterial function by alternating between the redox states of Cu^{+} and Cu^{2+} ions.[40,41] Free Cu^{+} and Cu^{2+} ions are highly redox active and produce hydroxyl radical by the Fenton-like reaction:[42]

$$\mathrm{Cu(II)}+\mathrm{H_2O_2} \rightleftarrows \mathrm{Cu(I)}+\cdot\mathrm{HO_2}+\mathrm{H^+} \quad (3)$$

$$\mathrm{Cu(I)}+\mathrm{H_2O_2} \rightarrow \mathrm{Cu(II)}+\mathrm{OH^-}+\cdot\mathrm{OH} \quad (4)$$

Thus, a small amount of soluble Cu can have a strong biological efficacy.

4.4. *In Vitro* and *in Vivo* Osteogenesis

Apart from the outstanding antibacterial activity, Cu element is essential for the metabolism of the skeleton. Although the exact function of Cu element in bone growth and development is unclear, it is well-known that the Cu element deficiency leads to bone abnormalities.[43] Mild Cu element deficiency contributes to bone defects characterized as osteoporotic-like lesions and bone fragility in humans and animals. As to human diseases, significant deficiencies in Cu element content have been found in osteoporotic patients compared with healthy people and the supplement of Cu element prevents spinal bone loss in postmenopausal women.[44,45] In Menke's syndrome and occipital horn syndrome, the deficiency of Cu element and its effects on the function of copper-dependent enzymes were observed.[46]

Other researchers have also studied the effect of Cu^{2+} ions on the proliferation and osteogenic differentiation of bone mesenchymal stem cells (MSCs) or preosteoblasts. Fromigué et al. have found the proliferation and differentiation processes of MSCs were regulated in an opposite manner by Cu^{2+} ions.[47] Rodriguez et al. indicated that cell proliferation decreased when human MSCs were cultured in a Cu-supplemented medium while their differentiation was enhanced.[48] It was also reported that Cu-containing bioactive glass scaffolds could promote the osteogenic differentiation of human bone marrow stromal cells by upregulation of osteogenic genes expression, including ALP, OCN, and osteopontin (OPN).[49] Cu bearing stainless steel has also been proved to stimulate the ALP activity and the osteogenic genes expression *in vitro* as well as enhance new bone formation around the implants *in vivo*.[50]

In the present study, the addition of Cu in the scaffolds had no significant influence on the proliferation of MC3T3-E1 cells. However, it led to a much higher level of the ALP activity, revealing that Cu^{2+} ions could enhance the differentiation of cultured preosteoblasts. The increase of ALP activity in the early stage is a marker of the differentiation toward osteoblasts while the formation of more mature phenotype and the advanced matrix mineralization can result in a subsequent decrease of ALP.[51,52] We demonstrated that the presence of Cu enhanced calcium deposition and bone matrix formation by the alizarin red S staining on day 14. We further observed the differentiation and mineralization of

preosteoblasts by examining the expression of bone-related gene expression. We found bone-related genes COL-I and OCN presented a significantly higher level of expression in the CMC/Alg/Cu scaffolds than in the CMC/Alg scaffolds after 14 days of culture. COL-I is vital in the maturation and mineralization of the bone matrix as a major protein constituting the bone matrix. OCN, a late-stage marker of osteoblast differentiation, triggers extracellular matrix deposition by its product.[53]

Osteoinductive ability of the scaffolds was further demonstrated by *in vivo* study. 3D restructure showed an increased amount of bone formation in the CMC/Alg/Cu scaffolds, and correspondingly, BMD was significantly higher. Masson's trichrome staining also showed there were more osteocytes and collagen in the CMC/Alg/Cu scaffolds. Thus, the addition of Cu into CMC/Alg scaffolds could enhance osteogenesis by promoting osteoblast differentiation and, in particular, mineralization.

Cu has been evidenced to facilitate angiogenesis decades ago. It is believed that Cu acts as an endogenous stimulator of angiogenesis to enhance migration and proliferation of endothelial cells.[54] Cu can accelerate wound healing by stimulating vascular endothelial growth factor (VEGF) expression.[55] In a study of Cu containing mesoporous bioactive glass (MBG), both Cu-MBG scaffolds and their ionic extracts stimulated hypoxia-inducible factor (HIF)-1α and VEGF expression in human bone marrow stromal cells.[49] This discovery is further confirmed in a study of graphene oxide–copper nanocomposite (GO-Cu) coated porous calcium phosphate (CaP) scaffolds.[56] The GO-Cu upregulated the expression of Hif-1α and enhanced the secretion of VEGF and bone morphometric protein 2 (BMP-2) in MSCs by activating the extracellular signal-regulated kinases 1/2 (Erk1/2) signaling pathway. The GO-Cu coated CaP cement scaffolds significantly promoted angiogenesis and osteogenesis in a calvarial defect rat model. In our study, we found that there were more vessels formed in the CMC/Alg/Cu scaffolds than in the CMC/Alg scaffolds at both weeks 2 and 4 after implantation *in vivo*. As angiogenesis is of significant importance in healing bone defects, the addition of Cu represents a feasible approach to promote bone healing.

Taken together, as Figure 7 shows, compared with the CMC/Alg scaffolds, the CMC/Alg/Cu scaffolds gradually released Cu^{2+} ions. The released Cu^{2+} ions promoted cell adhesion by activating focal adhesion and an actin cytoskeleton pathway and enhanced osteogenesis by increasing osteogenic genes expression, mineralization, and vessel formation. In addition, the release of Cu^{2+} ions also strengthened the antibacterial property of the scaffolds.

5. CONCLUSION

In this study, we developed an innovative approach to fabricate a novel type of Cu-containing natural polymer CMC/Alg scaffolds. The novelty lies in the incorporation of Cu nanoparticles into the CMC/Alg polymer mixture, enabling the controlled release of Cu ions to cross-link polymers for forming scaffolds and for making the scaffolds bear enhanced osteogenesis-promoting and bacteria-killing capabilities. By a series of *in vitro* and *in vivo* tests, we found that the Cu doped CMC/Alg scaffolds (CMC/Alg/Cu) had a good biocompatibility and promoted cell adhesion and osteogenesis by the release of Cu^{2+} ions. More importantly, the addition of Cu to the scaffolds significantly eradicated clinical

bacteria. Thus, the CMC/Alg/Cu scaffolds with multifunctional characteristics could be used to repair infected bone defects.

Supplementary Material

Refer to Web version on PubMed Central for supplementary material.

Acknowledgments

We appreciate the financial support from the National Key Research and Development Program of China (2016YFB0700800, 2017YFB0702604, 2016YFA0100900), the National Natural Science Foundation of China (21620102004 and 51673168), the Natural Science Foundation of Guangdong Province (2015A030312004), and the Science and Technology Planning Project of Guangzhou city (201604020110). Y. Zhu and C.M. are also thankful for the financial support from National Institutes of Health (CA195607).

References

1. Frink, M., Ruchholtz, S. Open Fractures: Initial Management. Springer; Berlin Heidelberg: 2016. p. 261-275.
2. Han F, Peter L, Lau ET, Thambiah J, Murphy D, Kagda FH. Reamer Irrigator Aspirator Bone Graft Harvesting: Complications and Outcomes in an Asian Population. Injury. 2015; 46(10):2042–2051. [PubMed: 26253387]
3. Karagozlu MZ, Kim SK. Chapter Twelve–Anticancer Effects of Chitin and Chitosan Derivatives. Adv Food Nutr Res. 2014; 72:215–225. [PubMed: 25081085]
4. Li LH, Li M, Li D, He P, Xia H, Zhang Y, Mao C. Chemical Functionalization of Bone Implants with Nanoparticle-Stabilized Chitosan and Methotrexate for Inhibiting both Osteoclastoma Formation and Bacterial Infection. J Mater Chem B. 2014; 2(36):5952–5961. [PubMed: 25177491]
5. Ngo DH, Kim SK. Chapter Two–Antioxidant Effects of Chitin, Chitosan, and Their Derivatives. Adv Food Nutr Res. 2014; 73:15–31. [PubMed: 25300540]
6. Lu Y, Li M, Li L, Wei S, Hu X, Wang X, Shan G, Zhang Y, Xia H, Yin Q. High-Activity Chitosan/Nano Hydroxyapatite/Zoledronic Acid Scaffolds for Simultaneous Tumor Inhibition, Bone Repair and Infection Eradication. Mater Sci Eng, C. 2018; 82:225–233.
7. Jayakumar R, Prabaharan M, Reis RL, Mano JF. Graft Copolymerized Chitosan-Present Status and Applications. Carbohydr Polym. 2005; 62(2):142–158.
8. Li X, Kong X, Zhang Z, Nan K, Li L, Wang X, Chen H. Cytotoxicity and Biocompatibility Evaluation of N,O-Carboxymethyl Chitosan/Oxidized Alginate Hydrogel for Drug Delivery Application. Int J Biol Macromol. 2012; 50(5):1299–1305. [PubMed: 22465755]
9. Müller WE, Neufurth M, Wang S, Tolba E, Schröder HC, Wang X. Morphogenetically Active Scaffold for Osteochondral Repair (Polyphosphate/Alginate/N,O-Carboxymethyl Chitosan). Eur Cells Mater. 2016; 31:174–190.
10. Sakai S, Yamada Y, Zenke T, Kawakami K. Novel Chitosan Derivative Soluble at Neutral PH and in-Situ Gellable via Peroxidase-Catalyzed Enzymatic Reaction. J Mater Chem. 2009; 19(2):230–235.
11. Venkatesan J, Kim SK. Chitosan Composites for Bone Tissue Engineering—An Overview. Mar Drugs. 2010; 8(8):2252–2266. [PubMed: 20948907]
12. Venkatesan J, Bhatnagar I, Manivasagan P, Kang KH, Kim SK. Alginate Composites for Bone Tissue Engineering: a Review. Int J Biol Macromol. 2015; 72:269–281. [PubMed: 25020082]
13. Huang Y, Yao M, Zheng X, Liang X, Su X, Zhang Y, Lu A, Zhang L. Effects of Chitin Whiskers on Physical Properties and Osteoblast Culture of Alginate Based Nanocomposite Hydrogels. Biomacromolecules. 2015; 16(11):3499–3507. [PubMed: 26393272]
14. He X, Liu Y, Yuan X, Lu L. Enhanced Healing of Rat Calvarial Defects with MSCs Loaded on BMP-2 Releasing Chitosan/Alginate/Hydroxyapatite Scaffolds. PLoS One. 2014; 9(8):e104061–e104069. [PubMed: 25084008]

15. Sajesh KM, Jayakumar R, Nair SV, Chennazhi KP. Biocompatible Conducting Chitosan/Polypyrrole-Alginate Composite Scaffold for Bone Tissue Engineering. Int J Biol Macromol. 2013; 62(3):465–471. [PubMed: 24080452]
16. Venkatesan J, Bhatnagar I, Kim SK. Chitosan-Alginate Biocomposite Containing Fucoidan for Bone Tissue Engineering. Mar Drugs. 2014; 12(1):300–316. [PubMed: 24441614]
17. Shi C, Pu X, Zheng G, Feng X, Yang X, Zhang B, Zhang Y, Yin Q, Xia H. An Antibacterial and Absorbable Silk-Based Fixation Material with Impressive Mechanical Properties and Biocompatibility. Sci Rep. 2016; 6:37418–37429. [PubMed: 27869175]
18. Iviglia G, Cassinelli C, Bollati D, Baino F, Torre E, Morra M, Vitale-Brovarone C. Engineered Porous Scaffolds for Periprosthetic Infection Prevention. Mater Sci Eng, C. 2016; 68:701–715.
19. Inzana JA, Schwarz EM, Kates SL, Awad HA. Biomaterials Approaches to Treating Implant-Associated Osteomyelitis. Biomaterials. 2016; 81:58–71. [PubMed: 26724454]
20. Gao J, Huang G, Liu G, Liu Y, Chen Q, Ren L, Chen C, Ding Z. A Biodegradable Antibiotic-Eluting PLGA Nanofiber-Loaded Deproteinized Bone for Treatment of Infected Rabbit Bone Defects. J Biomater Appl. 2016; 31(2):241–249. [PubMed: 27288462]
21. Ewald A, Käppel C, Vorndran E, Moseke C, Gelinsky M, Gbureck U. The Effect of Cu(II)-Loaded Brushite Scaffolds on Growth and Activity of Osteoblastic Cells. J Biomed Mater Res, Part A. 2012; 100(9):2392–2400.
22. D'Mello S, Elangovan S, Hong L, Ross RD, Sumner DR, Salem AK. Incorporation of Copper into Chitosan Scaffolds Promotes Bone Regeneration in Rat Calvarial Defects. J Biomed Mater Res, Part B. 2015; 103(5):1044–1049.
23. Ma Z, Ren L, Liu R, Yang K, Zhang Y, Liao Z, Liu W, Qi M, Misra RDK. Effect of Heat Treatment on Cu Distribution, Antibacterial Performance and Cytotoxicity of Ti-6A1–4V-SCu Alloy. J Mater Sci Technol (Shenyang, China). 2015; 31(7):723–732.
24. Ruparelia JP, Chatterjee AK, Duttagupta SP, Mukherji S. Strain Specificity in Antimicrobial Activity of Silver and Copper Nanoparticles. Acta Biomater. 2008; 4(3):707–716. [PubMed: 18248860]
25. Midander K, Cronholm P, Karlsson HL, Elihn K, Möller L, Leygraf C, Wallinder IO. Surface Characteristics, Copper Release, and Toxicity of Nano- and Micrometer-Sized Copper and Copper(II) Oxide Particles: A Cross-Disciplinary Study. Small. 2009; 5(3):389–399. [PubMed: 19148889]
26. Mudunkotuwa IA, Pettibone JM, Grassian VH. Environmental Implications of Nanoparticle Aging in the Processing and Fate of Copper-Based Nanomaterials. Environ Sci Technol. 2012; 46(13): 7001–7010. [PubMed: 22280489]
27. Shannon RD. Revised Effective Ionic Radii and Systematic Studies of Interatomic Distances in Halides and Chalcogenides. Acta Crystallogr, Sect A: Cryst Phys, Diffr, Theor Gen Crystallogr. 1976; 32(5):751–767.
28. Lin YH, Liang HC, Chung CK, Chen MC, Sung HW. Physically Crosslinked Alginate/N,O-Carboxymethyl Chitosan Hydrogels with Calcium for Oral Delivery of Protein Drugs. Biomaterials. 2005; 26(14):2105–2113. [PubMed: 15576185]
29. Pampaloni F, Reynaud EG, Stelzer EHK. The Third Dimension Bridges the Gap between Cell Culture and Live Tissue. Nat Rev Mol Cell Biol. 2007; 8(10):839–845. [PubMed: 17684528]
30. Cukierman E, Pankov R, Stevens DR, Yamada KM. Taking Cell-Matrix Adhesions to the Third Dimension. Science. 2001; 294(5547):1708–1712. [PubMed: 11721053]
31. Ren N, Li J, Qiu J, Sang Y, Jiang H, Boughton RI, Huang L, Huang W, Liu H. Nanostructured Titanate with Different Metal Ions on the Surface of Metallic Titanium: a Facile Approach for Regulation of rBMSCs Fate on Titanium Implants. Small. 2014; 10(15):3169–3180. [PubMed: 24706634]
32. Yang D, Lü X, Hong Y, Xi T, Zhang D. The Molecular Mechanism of Mediation of Adsorbed Serum Proteins to Endothelial Cells Adhesion and Growth on Biomaterials. Biomaterials. 2013; 34(23):5747–5758. [PubMed: 23660250]
33. Carragher NO, Frame MC. Focal Adhesion and Actin Dynamics: a Place where Kinases and Proteases Meet to Promote Invasion. Trends Cell Biol. 2004; 14(14):241–249. [PubMed: 15130580]

34. Sowjanya JA, Singh J, Mohita T, Sarvanan S, Moorthi A, Srinivasan N, Selvamurugan N. Biocomposite Scaffolds Containing Chitosan/Alginate/Nano-Silica for Bone Tissue Engineering. Colloids Surf, B. 2013; 109(9):294–300.
35. Zhang H, Ji Z, Xia T, Meng H, Lowkam C, Liu R, Pokhrel S, Lin S, Wang X, Liao YP, et al. Use of Metal Oxide Nanoparticle Band Gap to Develop a Predictive Paradigm for Oxidative Stress and Acute Pulmonary Inflammation. ACS Nano. 2012; 6(5):4349–4368. [PubMed: 22502734]
36. Studer AM, Limbach LK, Van Duc L, Krumeich F, Athanassiou EK, Gerber LC, Moch H, Stark WJ. Nanoparticle Cytotoxicity Depends on Intracellular Solubility: Comparison of Stabilized Copper Metal and Degradable Copper Oxide Nanoparticles. Toxicol Lett. 2010; 197(3):169–174. [PubMed: 20621582]
37. Jo HJ, Choi JW, Lee SH, Hong SW. Acute Toxicity of Ag and CuO Nanoparticle Suspensions against Daphnia Magna: the Importance of Their Dissolved Fraction Varying with Preparation Methods. J Hazard Mater. 2012; 227–228(5):301–308.
38. Ning C, Wang X, Li L, Zhu Y, Li M, Yu P, Zhou L, Zhou Z, Chen J, Tan G, et al. Concentration Ranges of Antibacterial Cations for Showing the Highest Antibacterial Efficacy but the Least Cytotoxicity against Mammalian Cells: Implications for a New Antibacterial Mechanism. Chem Res Toxicol. 2015; 28(9):1815–1822. [PubMed: 26258952]
39. Li M, Ma Z, Zhu Y, Xia H, Yao M, Chu X, Wang X, Yang K, Yang M, Zhang Y, et al. Toward a Molecular Understanding of the Antibacterial Mechanism of Copper-Bearing Titanium Alloys against Staphylococcus Aureus. Adv Healthcare Mater. 2016; 5(5):557–566.
40. Abou Neel EA, Ahmed I, Pratten J, Nazhat SN, Knowles JC. Characterisation of Antibacterial Copper Releasing Degradable Phosphate Glass Fibres. Biomaterials. 2005; 26(15):2247–2254. [PubMed: 15585226]
41. Applerot G, Lellouche J, Lipovsky A, Nitzan Y, Lubart R, Gedanken A, Banin E. Understanding the Antibacterial Mechanism of CuO Nanoparticles: Revealing the Route of Induced Oxidative Stress. Small. 2012; 8(21):3326–3337. [PubMed: 22888058]
42. Wang Z, von dem Bussche A, Kabadi PK, Kane AB, Hurt RH. Biological and Environmental Transformations of Copper-Based Nanomaterials. ACS Nano. 2013; 7(10):8715–8727. [PubMed: 24032665]
43. Strain JJ. A Reassessment of Diet and Osteoporosis — Possible Role for Copper. Med Hypotheses. 1988; 27(4):333–338. [PubMed: 3067062]
44. Strause L, Saltman P, Smith KT, Bracker M, Andon MB. Spinal Bone Loss in Postmenopausal Women Supplemented with Calcium and Trace Minerals. J Nutr. 1994; 124(7):1060–1064. [PubMed: 8027856]
45. Eaton-Evans J. Osteoporosis and the Role of Diet. Br J Biomed Sci. 1994; 51(4):358–370. [PubMed: 7756943]
46. Kodama H, Murata Y. Molecular Genetics and Pathophysiology of Menkes Disease. Pediatr Int. 1999; 41(4):430–435. [PubMed: 10453200]
47. Fromigué O, Marie PJ, Lomri A. Bone Morphogenetic Protein-2 and Transforming Growth Factor-Beta2 Interact to Modulate Human Bone Marrow Stromal Cell Proliferation and Differentiation. J Cell Biochem. 1998; 68(4):411–426. [PubMed: 9493905]
48. Rodríguez JP, Ríos S, González M. Modulation of the Proliferation and Differentiation of Human Mesenchymal Stem Cells by Copper. J Cell Biochem. 2002; 85(1):92–100. [PubMed: 11891853]
49. Wu C, Zhou Y, Xu M, Han P, Chen L, Chang J, Xiao Y. Copper-Containing Mesoporous Bioactive Glass Scaffolds with Multifunctional Properties of Angiogenesis Capacity, Osteostimulation and Antibacterial Activity. Biomaterials. 2013; 34(2):422–433. [PubMed: 23083929]
50. Ren L, Wong HM, Yan CH, Yeung KW, Yang K. Osteogenic Ability of Cu-Bearing Stainless Steel. J Biomed Mater Res, Part B. 2015; 103(7):1433–1444.
51. Sugawara Y, Suzuki K, Koshikawa M, Ando M, Iida J. Necessity of Enzymatic Activity of Alkaline Phosphatase for Mineralization of Osteoblastic Cells. Jpn J Pharmacol. 2002; 88(3):262–269. [PubMed: 11949880]
52. Jaiswal N, Haynesworth SE, Caplan AI, Bruder SP. Osteogenic Differentiation of Purified, Culture-Expanded Human Mesenchymal Stem Cells in Vitro. J Cell Biochem. 1997; 64(2):295–312. [PubMed: 9027589]

53. Li M, He P, Wu Y, Zhang Y, Xia H, Zheng Y, Han Y. Stimulatory Effects of the Degradation Products from Mg-Ca-Sr Alloy on the Osteogenesis through Regulating ERK Signaling Pathway. Sci Rep. 2016; 6:32323–32335. [PubMed: 27580744]

54. Hu GF. Copper Stimulates Proliferation of Human Endothelial Cells Under Culture. J Cell Biochem. 1998; 69(3):326–335. [PubMed: 9581871]

55. Sen CK, Khanna S, Venojarvi M, Trikha P, Ellison EC, Hunt TK, Roy S. Copper-Induced Vascular Endothelial Growth Factor Expression and Wound Healing. Am J Physiol: Heart Circ Physiol. 2002; 282(5):H1821–1827. [PubMed: 11959648]

56. Zhang W, Chang Q, Xu L, Li G, Yang G, Ding X, Wang X, Cui D, Jiang X. Graphene Oxide-Copper Nanocomposite-Coated Porous CaP Scaffold for Vascularized Bone Regeneration via Activation of Hif-1α. Adv Healthcare Mater. 2016; 5(11):1299–1309.

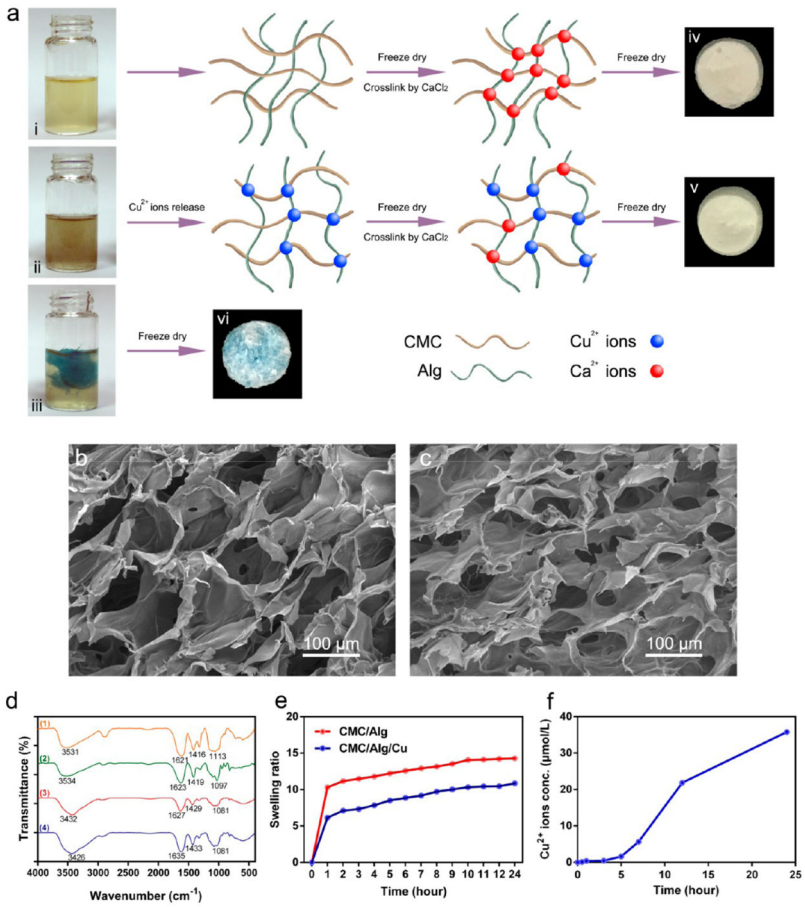

Figure 1.

Preparation and characterization of scaffolds. (a) Schematic illustration of the preparation of the scaffolds. i, ii, and iii represent CMC/Alg solution, CMC/Alg solution containing 1 mmol/L Cu nanoparticles, and CMC/Alg solution containing 1 mmol/L directly added Cu^{2+} solution. iv, v, and vi are CMC/Alg scaffold, CMC/Alg/Cu scaffold, and CMC/Alg/Cu^{2+} scaffold cross-linked by directly added Cu^{2+} solution and derived from the freeze-drying of solutions i, ii, and iii, respectively. (b, c) SEM images of the CMC/Alg/Cu (b) and CMC/Alg (c) scaffolds. (d) FTIR spectra of the scaffolds. 1, 2, 3, and 4 represent CMC, Alg, CMC/Alg scaffold, and CMC/Alg/Cu scaffold, respectively. (e) Swelling behavior of the scaffolds immersed in PBS. (f) Release of Cu^{2+} ions from the CMC/Alg/Cu scaffold immersed in PBS.

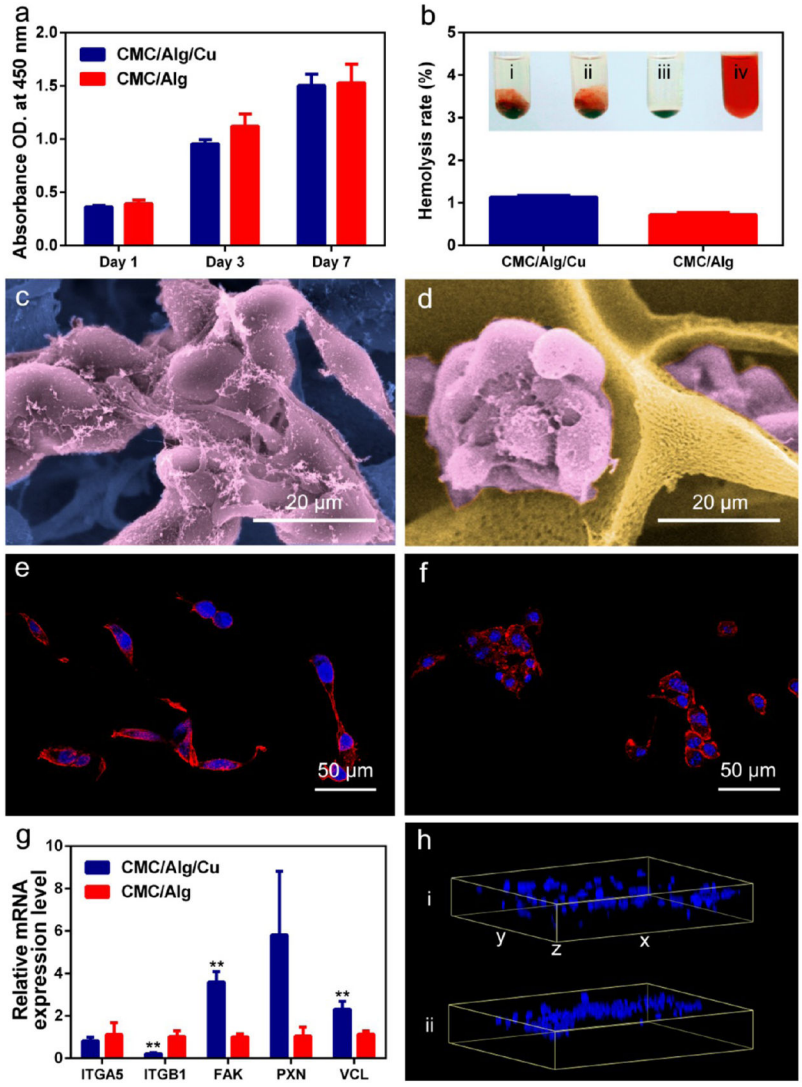

Figure 2.

Biocompatibility and cell adhesion of the scaffolds. (a) Proliferation of preosteoblasts in the scaffolds after 1, 3, and 7 days of incubation measured by the colorimetric CCK-8 assay. (b) Hemolysis rate (HR) tests of the scaffolds. Insets i, ii, iii, and iv represent CMC/Alg/Cu scaffold, CMC/Alg scaffold, negative control (saline), and positive control (DI water), respectively. (c, d) SEM observation of preosteoblasts adhered in the CMC/Alg/Cu (c) and CMC/Alg (d) scaffolds. Cells showed the presence of obvious filopodia in the CMC/Alg/Cu scaffold compared with CMC/Alg scaffolds. (e, f) Fluorescence staining of cytoskeleton in the CMC/Alg/Cu (e) and CMC/Alg (f) scaffolds. More typical actin proteins of microfilament structures were stained by phalloidin in the CMC/Alg/Cu scaffold. (g) The relative expression levels of genes related to cell adhesion in the scaffolds. Each value is the mean ± standard deviation of triplicate determinations; $*p < 0.05$, $**p < 0.01$ compared with CMC/Alg scaffolds. (h) The 3D distribution of the cells labeled with DAPI in the scaffolds. i and ii represent CMC/Alg/Cu and CMC/Alg scaffolds, respectively. This data suggests that preosteoblasts spread evenly throughout the CMC/Alg/Cu scaffold.

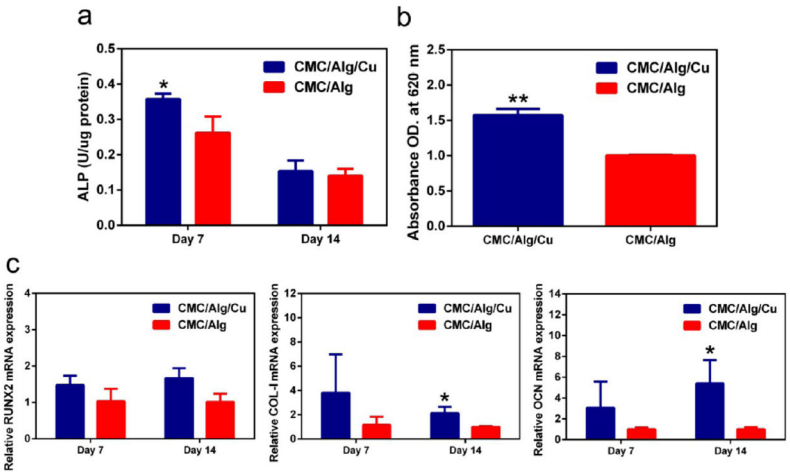

Figure 3.

In vitro osteogenesis capability of the scaffolds. (a) The ALP activity of the scaffolds on day 7 and 14. ALP level was significantly high in the CMC/Alg/Cu scaffolds on day 7 compared to CMC/Alg scaffolds and then decreased. (b) The extracellular calcium nodules were stained by alizarin red S, and the calcium deposition in the CMC/Alg/Cu scaffolds, represented by the absorbance at 620 nm, was significantly higher in the CMC/Alg/Cu scaffolds than that in the CMC/Alg scaffolds on day 14. (c) Relative expression of osteogenesis-related genes (left: RUX2; middle: Collagen I; right: OCN) after the preosteoblastic cells were cultured for 14 days. The expression level of COL-1 and OCN was significantly higher in CMC/Alg/Cu scaffolds than in CMC/Alg scaffolds. Each value is the mean ± standard deviation of triplicate determinations; $*p < 0.05$, $**p < 0.01$ compared with CMC/Alg scaffolds.

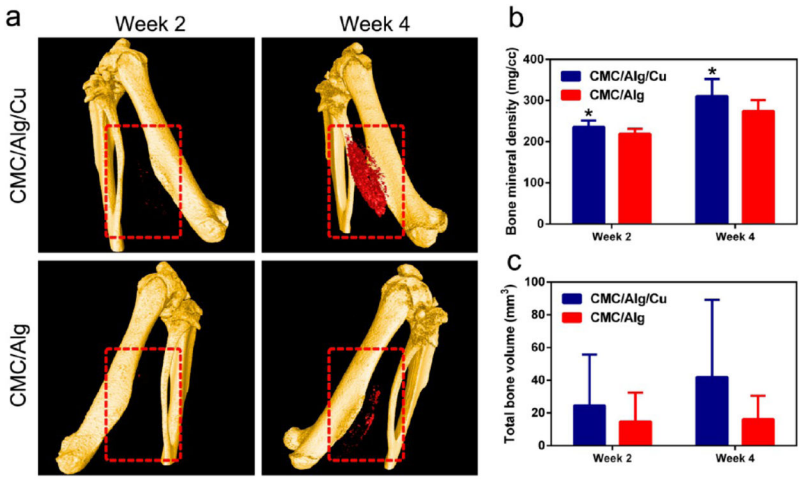

Figure 4.

Osteoinductive ability of the scaffolds *in vivo*. (a) Micro-CT 3D reconstruction models of the newly formed bone (red color) in the CMC/Alg/Cu and CMC/Alg scaffolds (highlighted by the red square) after 2 and 4 weeks postoperatively. Bone formation was found in the CMC/Alg/Cu scaffolds at week 2 and obviously increased at week 4. However, only slight bone formation was observed in the CMC/Alg even at week 4. (b) Bone mineral density (BMD) of the formed bone in the scaffolds. BMD was significantly higher in the CMC/Alg/Cu scaffolds than in the CMC/Alg scaffolds after 2 and 4 weeks of implantation. (c) Total bone volume (TBV) in the scaffolds. TBV was higher in the CMC/Alg/Cu scaffold than in the CMC/Alg scaffolds at both weeks 2 and 4. Each value is the mean ± standard deviation; $*p < 0.05$, $**p < 0.01$ compared with CMC/Alg scaffolds.

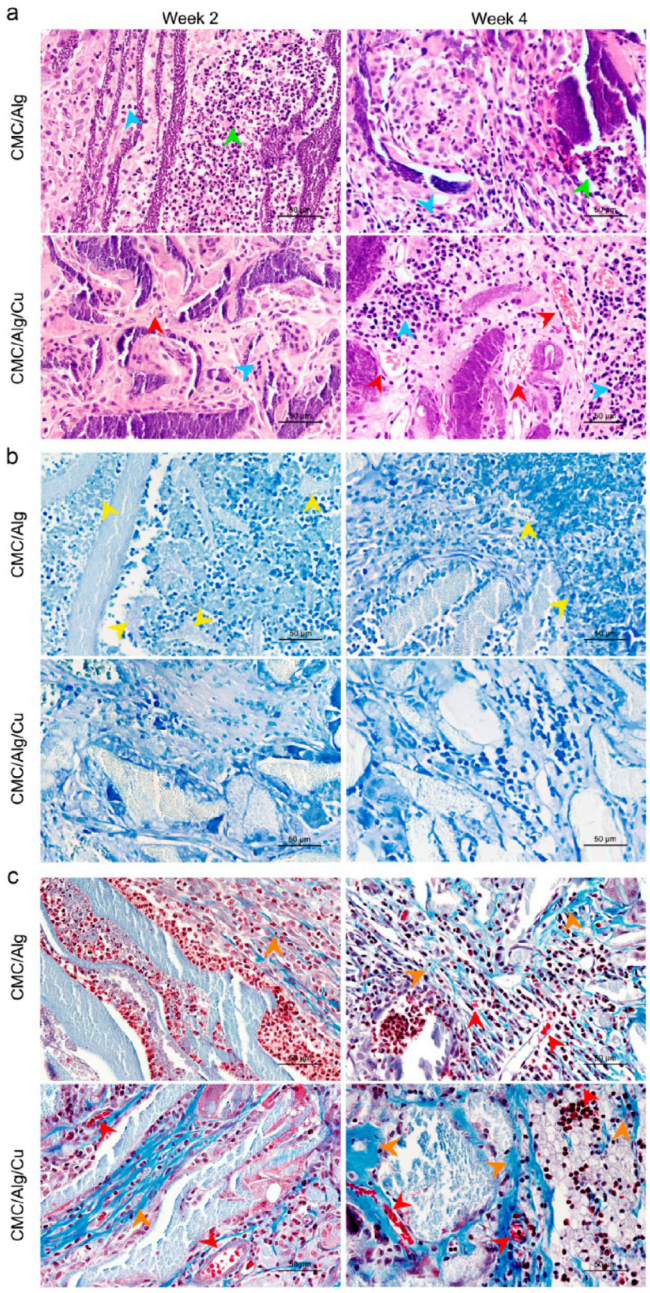

Figure 5.

Histological photographs of the harvested samples. (a) H&E staining showing that there were no lobulated neutrophils (green arrows) in the CMC/Alg/Cu scaffolds. In the CMC/Alg scaffolds, the number of lobulated neutrophils was high at 2 weeks postoperation and then decreased after 4 weeks. Osteocytes (blue arrows) were seen in both scaffolds after 2 weeks of implantation, and their number increased after 4 weeks. There were more osteocytes in the CMC/Alg/Cu scaffolds. Vessels (red arrows) were found in the CMC/Alg/Cu scaffolds at week 2 and then significantly increased at week 4. Almost no vessels were formed in the CMC/Alg scaffolds. (b) Giemsa staining showing that no obvious *S. aureus* (yellow arrows)

could be observed in the CMC/Alg/Cu scaffolds. A lot of *S. aureus* bacteria were seen at week 2, and then, the number of the bacteria decreased at week 4 in the CMC/Alg scaffolds. (c) Masson's trichrome staining showing that collagen (orange arrows) could be observed in both scaffolds after 2 weeks of implantation, and its amount was increased after 4 weeks of implantation. In the CMC/Alg/Cu scaffolds, more collagen was found.

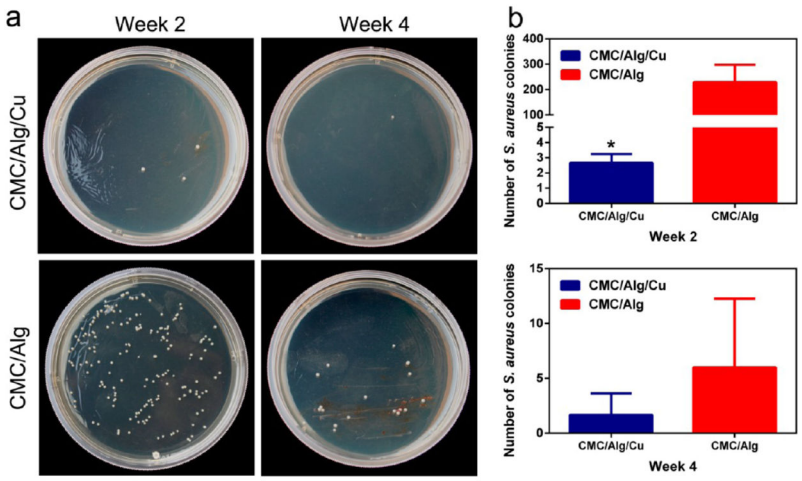

Figure 6.

Antibacterial properties of the scaffolds *in vivo*. (a) The number of clinically relevant *S. aureus* bacterial colonies after bacteria from the harvested samples were cultured for 24 h after 2 and 4 weeks of implantation. (b) *In vivo* antibacterial rate of the two scaffolds at week 2 (top) and week 4 (bottom). The CMC/Alg/Cu scaffolds showed a significantly higher antibacterial activity *in vivo* at both weeks 2 and 4 than the CMC/Alg scaffolds. Each value is the mean ± standard deviation; $*p < 0.05$, $**p < 0.01$ compared with CMC/Alg scaffolds.

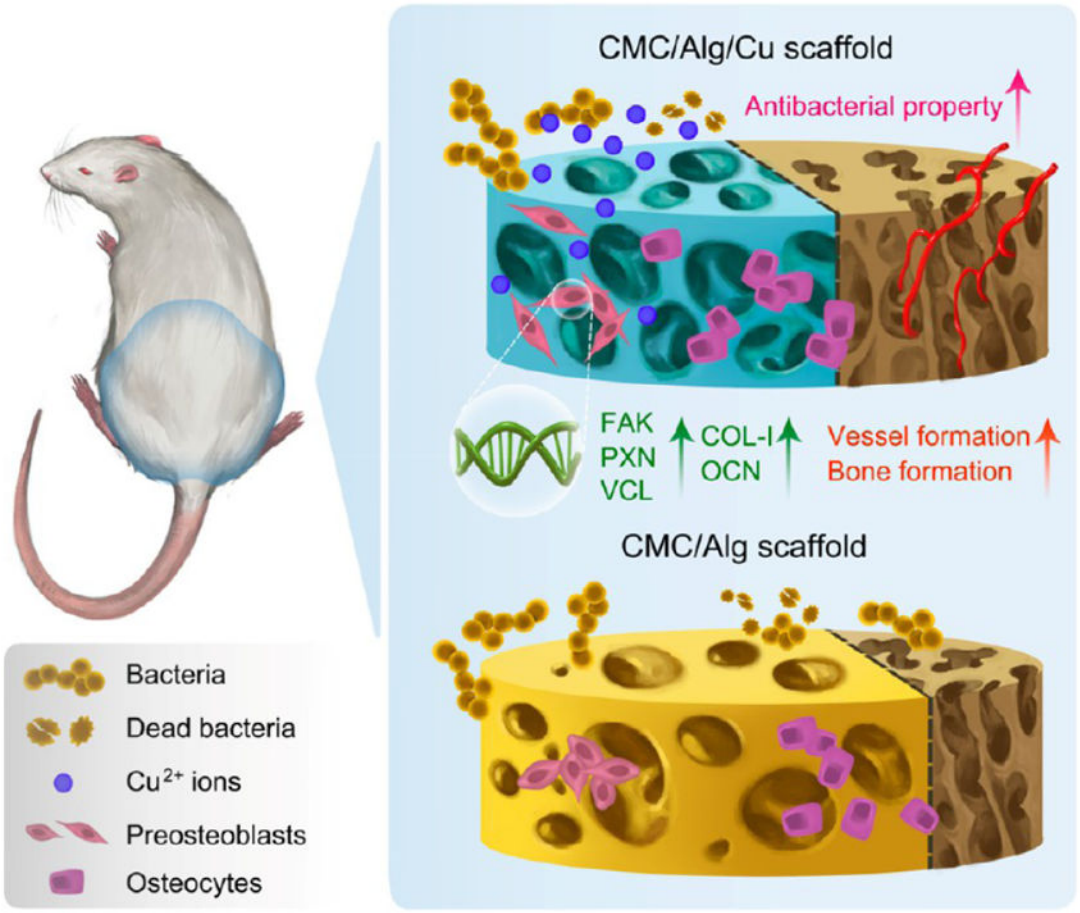

Figure 7.
Schematic illustration of the antibacterial and osteogenic processes *in vivo*.

Table 1

Primer Sequences Used for RT-qPCR of Adhesion-Related Genes Expression

	primer sequence	
gene	**forward**	**reverse**
ITGNA5	5′-AGCAACTGCACCTCCAACTACA-3′	5′-ACACTTGGCTTCAGGGCATT-3′
ITGB1	5′-TTGGTCAGCAACGCATATCTG-3′	5′-CAGCAAAGTGAAACCCAGCAT-3′
FAK	5′-GCAATGGAACGAGTATTAAAGGTCTT-3′	5′-GGCCACGTGCTTTACTTTGTG-3′
PXN	5′-CTCTGAACTTGACCGGCTGTTA-3′	5′-CCCCCCAAGGGAGTGTTATT-3′
VCL	5′-GTGGCGACGGCACTACAGA-3′	5′-ACCGACTCCACGGTCATCTACT-3′
GAPDH	5′-CATGGCCTTCCGTGTTCCTA-3′	5′-CCTGCTTCACCACCTTCTTGAT-3′

Table 2

Primer Sequences Used for RT-qPCR of Osteogenesis-Related Genes Expression

	primer sequence	
gene	**forward**	**reverse**
RUNX2	5′-TCCAACCCACGAATGCACTA-3′	5′-GAAGGGTCCACTCTGGCTTTG-3′
COL-I	5′-GCAGGGTTCCAACGATGTTG-3′	5′-AGGAACGGCAGGCGAGAT-3′
OCN	5′-CAATAAGGTAGTGAACAGAC-3′	5′-CTTCAAGCCATACTGGTCT-3′
GAPDH	5′-CATGGCCTTCCGTGTTCCTA-3′	5′-CCTGCTTCACCACCTTCTTGAT-3′